An X-ray Diffraction Study of the Structure of Vitreous P2O5

Uwe Hoppe, Günter Walter, Rainer Kranold, and Dörte Stachel^a

Universität Rostock, Fachbereich Physik, D-18051 Rostock

^a Friedrich-Schiller-Universität Jena, Otto-Schott-Institut, Chemisch-Geowissenschaftliche Fakultät, D-07743 Jena

Z. Naturforsch. 53a, 93-104 (1998); received December 22, 1997

Recently, the lengths of the two P-O bonds in the PO_4 tetrahedron were obtained by neutron diffraction of high real-space resolution. By use of the present X-ray diffraction experiments, the P-P distance belonging to pairs of corner-linked PO_4 units is determined. Using this length of (294 \pm 2) pm and taking into account the P-O bond distance to the bridging oxygen atom of 158 pm, a mean P-O-P angle of 137° \pm 3° is calculated. The reverse Monte Carlo simulations fit the neutron and X-ray structure factors. The P-O-P angle distribution obtained this way possesses a mean angle of 141°. An interpretation of the first scattering peaks is presented by analysing the occupancy and the distances of various coordination shells by use of model configurations. The low occupancy of the first shells allows the application of the schematic hole model of Dixmier. The first X-ray diffraction peak at 13 nm $^{-1}$ is related to the P-P2nd shell, the shoulder at 20 nm $^{-1}$ arises from the P-O2nd shell. The most similar crystalline structure with vitreous P_2O_5 is the orthorhombic P_2O_5 , form II. But it has more effectively orientated terminal oxygen atoms and, thus, a higher packing than the glass.

Key words: Vitreous P₂O₅; X-ray Diffraction; Short-range Order; Reverse Monte Carlo.

1. Introduction

Spectroscopic methods have confirmed that vitreous $(v-)P_2O_5$ forms corner-sharing PO₄ tetrahedra [1-5]. Since the valency of the phosphorus atom is 5, one of the oxygen of the PO₄ unit (O_T or O_{DB}) is not shared with an adjacent tetrahedron but is doubly bonded with the P atom. Using the high real-space resolution of diffraction experiments, which is available with neutron spallation sources, the P-O peak is well resolved into two separate contributions [6]. The P-O bond length to the bridging O atom (O_B) is (158.1 ± 0.3) pm, that to the O_T is (143.2 ± 0.5) pm. Even the O-O peak at 252 pm consists of two contributions, those belonging to the O_B-O_B and the O_B-O_T tetrahedral edges [6]. However, in the data resulting from the neutron diffraction measurements the weight of the partial P-P correlations is small. Since P atoms scatter the X-rays more strongly than O atoms, an X-ray diffraction experiment is quite profitable for studying the mutual order of the PO₄ units. The real-space correlation function, T(r), resulting from our present X-ray diffraction experiment on v-P₂O₅ was already shown in [7]. The data include a clear P-P peak at ≈ 0.3 nm. From this P-P distance and the P-O_B bond length, the P-O_B-P bridging angle can be obtained. However, an analysis of those structural features which exceed the shortrange order is a complex task, and it requires some modelling. The reverse Monte Carlo (RMC) technique [8] is highly effective in combining the structural information from the neutron and X-ray scattering data of different contrast, which are now available, and other useful constraints. Up to now other modelling techniques, e.g. Molecular Dynamics, have not been successful in simulating phosphate glass structures. Corresponding work [9, 10] resulted in quite unrealistic distributions of the links between the PO₄ units.

The early part of scattering curves of disordered materials, i.e. the Q-range up to 30 nm⁻¹, gives information about the medium-range structure [11-14]. Q is the magnitude of the scattering vector with $Q = 4\pi/\lambda \sin \theta$, where 2θ is the scattering angle and λ the radiation wavelength. The first large peak in the structure factors, S(O), sometimes called a main peak, is split in the neutron $S_N(Q)$ data for $v-P_2O_5$ but not in those for $v-SiO_2$ [15]. The same behaviour is apparent in the X-ray $S_X(Q)$ data for v-P₂O₅ [7]. Therefore, the structure of P₂O₅ glass was suggested [16] to consist dominantly of parallel sheets but flattened if compared with those in the P_2O_5 , form III crystal [17]. Two different periods of atomic density fluctuations, one being effective in the direction of the sheets and one perpendicularly to them, should produce the specific scattering effect observed [16]. However, the other known crystalline forms possess different network features which may exist in the glass, as well. The first structure

Reprint requests to Dr. U. Hoppe; Fax: +493814981726.

is built up of P_4O_{10} molecules [18], and the P_2O_5 , form II [19] has a 3-dimensional network. In order to examine the similarity of the main features of the glass structure with any of the crystalline forms, glass-like structure factors of the related crystals will be calculated. The RMC simulations will help in analyses of the origin of the first diffraction peaks and of other features of the network structure of ν - P_2O_5 .

A network of threefold-linked PO_4 units possesses more structural variability than that of fourfold-linked units, e.g. the SiO_4 tetrahedra in silica. In [6] it was emphasized that the environments of the O_T atoms are sensitive to the various ways of packing on the P_2O_5 networks. Here, additionally, the numbers and distances of the first and second P neighbours of the PO_4 units will be considered. Elliott has analysed the pattern of prepeaks in front of the principal peak [12]. The position Q_p of a principal peak with

$$Q_{\rm p} \approx 7.7/r_1 \tag{1}$$

is defined by the shortest distance, r_1 . Such a peak is the first one in case of a system with a dense random packing of hard spheres with a separation distance of r_1 [20]. Prepeaks at lower Q, which occationally occur, are a signature for a specific construction of the first several coordination spheres which differ from a dense random packing.

2. Experimental

The details of the sample preparation were described in [5, 21]. The raw material was a powder of P_4O_{10} (p.A. Merck) which was melted in a sealed and evacuated silica ampoule for two hours at 1050°C. The P₂O₅ glass prepared in that way was nearly free of water [21]. By use of an electron microprobe X-ray analyzer, a small contamination of the P₂O₅ glass with silica was found near the surface of the ampoule [22]. But in the larger middle part of the ampoule no silica was detectable. Material from this region was used for the measurements. Pieces of v-P₂O₅ were stored under paraffin oil for the sample transport. A silica capillary of about 1.3 mm diameter and 15 µm wall thickness was the container for the X-ray measurements. A coarse-grained powder of the sample material just crushed was filled into the capillary which was subsequently sealed by paraffin. This procedure was performed very quickly (less than half a minute) without the use of a glove box. The mass density of the glass was taken from an extrapolation of values from

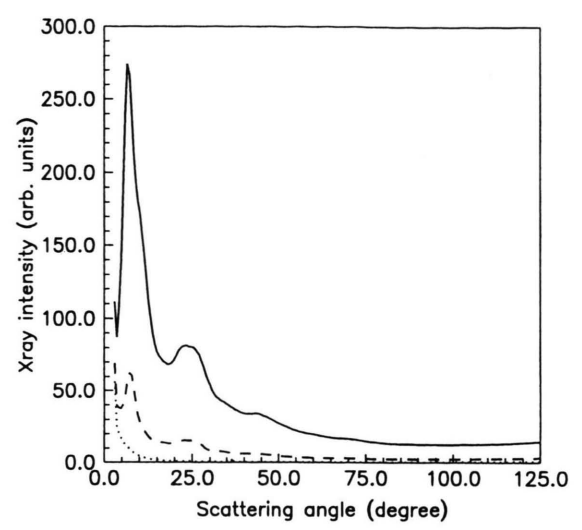


Fig. 1. Raw X-ray intensities of the filled capillary (solid line), the empty capillary (dashed line), and the background intensity (dotted line).

various series of ultraphosphate glasses (2.445 g/cm³)

The X-ray diffraction experiment was performed on a horizontal goniometer in a step scan mode using an interval of scattering angle, 2θ , from 3° to 132° with $\Delta\theta=0.3^\circ$. The Ag K $_\alpha$ radiation used allows to obtain the intensity in a Q-range from 6 to 202 nm $^{-1}$. A graphite crystal monochromator was positioned in the incident beam.

In case of cylindrical sample containers, the data processing requires the measurement of the full and the empty capillary, and of the background. Figure 1 shows the three measuring curves, where at every point in the sample scan 150,000 impulses were recorded. The angular dependence of the absorption coefficients was taken into account by numerical integration [23] using the beam profile at the sample position and the transmission coefficient measured for the filled capillary. Any error in subtracting the background of air scattering only affects the first measuring points. A more subtle problem is the elimination of the coherent scattering produced by the silica container. The reliability of the procedure here applied was successfully tested for other glassy materials, comparing the result obtained by this technique with that from the use of a slap-shaped sample [23].

After performing the polarization correction, the intensity curve was normalized by the Krogh-Moe method [24]. For the coherent component in the structure-independent scattering the sum of squares of the atomic

scattering factors $f_i(Q)$, taken from [25], was used with i being the sort of atoms. The Compton scattering was obtained by the analytical expression given by Smith et al. [26]. Finally, the total Faber-Ziman structure factor, $S_X(Q)$, was calculated by

$$S_{X}(Q) = \left\{ I(Q) - \left[\left\langle f_{i}(Q)^{2} \right\rangle - \left\langle f_{i}(Q) \right\rangle^{2} \right] \right\} / \left\langle f_{i}(Q) \right\rangle^{2}, (2)$$

where I(Q) is the normalized intensity after subtracting the Compton scattering and $\langle ... \rangle$ denotes an averaged value with respect to the sample composition. The $S_X(Q)$ function is shown in Fig. 4, where it is compared with the model function of the RMC simulations.

3. Modelling Procedures

3.1. Models Based on Crystalline Structures

For a first idea about the packing in a glassy network, models constructed from structural elements of the related crystals can be used. The calculations of glassy-like structure factors, $S_{\rm mod}(Q)$, on the basis of the local environments of the atoms in the crystals are similar to those described in [27]. The crystalline orientations are neglected in the $S_{\rm mod}(Q)$ functions by using the Debye formula in the scalar form with

$$S_{\text{mod}}(Q) = 1 + \sum_{i} c_{j} \int_{0}^{L+W} \frac{f_{i}(Q)f_{j}(Q)}{\langle f_{i}(Q) \rangle^{2}}$$

$$D_{ij}(r)F(r) \frac{\sin(Qr)}{Qr}$$

$$\exp[-0.5Q^{2}l(r)^{2}]dQ. \tag{3}$$

Value c_i is the molar fraction of atoms of sort *i*. The reduced functions $D_{ij}(r)$ of the partial radial distributions, $RDF_{ij}(r)$, of the discret pair distances in the crystal structures are diminished by the average atomic density, ρ_j , of atoms of sort *j* with

$$D_{ii}(r) = RDF_{ii}(r) - 4\pi r^2 \rho_i.$$
 (4)

 $l(r) = z \cdot r$ is the root mean squares displacement. It grows with the distance, which reflects the increasing disorder of atomic positions which are affected by distortions of bonds and bond angles. The value z was chosen to yield the width of the nearest-neighbour peak of the P-O bond in the glass. The lack of long-range correlations required for a suitable glass model was introduced by multiplying the $D_{ij}(r)$ data with an arbitrary function

F(r) which changes smoothly from unity at low r to zero at large distances:

$$F(r) = 1$$
 for $r < L - W$,
 $F(r) = 0$ for $r > L + W$,
 $F(r) = 1 - \sin^2 \left[\pi (r - L + W) / 4W \right]$ (5)
for $L - W \le r \le L + W$.

The values L and W were introduced for limiting the three ranges of different behaviour. L can be called a mean correlation length. Thus, in a small sphere of first neighbour distances, the short-range order of the crystal structure is preserved. This area is surrounded by a shell of diminished distance correlations. In order to avoid the scattering effect of the mode-shape, the shell is embedded in an environment of the mean atomic density.

3.2. The Reverse Monte Carlo Method

The RMC method is a tool for studying the 3-dimensional structure of disordered matter on the basis of the pair distance information which is mainly obtained by diffraction experiments [8]. Instead of the minimization of the system energy, as in the Metropolis Monte Carlo (MMC) method, here the criterion for the improvement of the atomic configuration in the model box is the agreement of the model and the experimental structure factors. Thus, a sum χ^2 of differences is calculated by

$$\chi^{2} = \sum [S_{\text{mod}}(Q_{i}) - S_{\text{exp}}(Q_{i})]^{2},$$
 (6)

where several S(Q) data, e.g. $S_N(Q)$ and $S_X(Q)$, can be used simultaneously. χ^2 is minimized by moving arbitrary atomic positions. The new position will be accepted in case of $\chi_n^2 < \chi_{n-1}^2$, where n-1 denotes the move accepted just before. Different from a simple relaxation, a probability $p = \exp(-(\chi_n^2 - \chi_0^2)/s)$ determines, which of the unfavourable moves has to accepted, as well. This probability is analogous to the factor $\exp(-U/kT)$ used in the MMC approach. The value s has a similar meaning as the temperature factor. It determines the equilibrium level about which χ^2 will fluctuate finally. According to the periodic boundary conditions used, no surface problems have to be considered. Information about the nearest neighbours, extracted from spectroscopic or other methods, can be profitably exploited in the simulations. Different from the program code of McGreevy et al. [28], in our procedure the constraints have no influence on χ^2 . Low-r limits of separation distances of the various atom pairs and maxima of the coordination numbers are defined. Subroutines for a first and second neighbour check are supplied.

The following are the constraints used in our RMC simulations for $v-P_2O_5$. The particle density of the 1400 atoms in the cubic box fits the expected value. The starting configuration is a statistical ensemble of the desired stoichiometric mixture of atoms. No specific method is in use which builds up a topology consistent with 3-connected units. In each step, the new atomic positions were checked with respect to the separation distances and coordination constraints. Unreasonable positions were rejected. Each of the P atoms was allowed to attach at most four oxygen neighbours. Only three of these O atoms in the PO₄ unit can form a P-O-P bridge. Edge-sharing PO₄ units are avoided. The breakage of P-O bonds was hampered compared with their formation by setting the probability $p \to 0$ in the first of cases. For improvement of the accuracy of the results, the model functions were obtained from five different RMC configurations.

4. Results

4.1. Fit of Parameters of the Nearest-neighbour Distances

Information about the short-range order has been extracted by modelling the nearest-neighbour peaks simultaneously in both real-space correlation functions, $T_N(r)$ and $T_X(r)$, which result from the $S_N(Q)$ and $S_X(Q)$ data by

$$T(r) = 4\pi r \rho_0 + 2/\pi \int_0^{Q_{\text{max}}} [S(Q) - 1]$$

$$\sin(Qr) Q dQ. \tag{7}$$

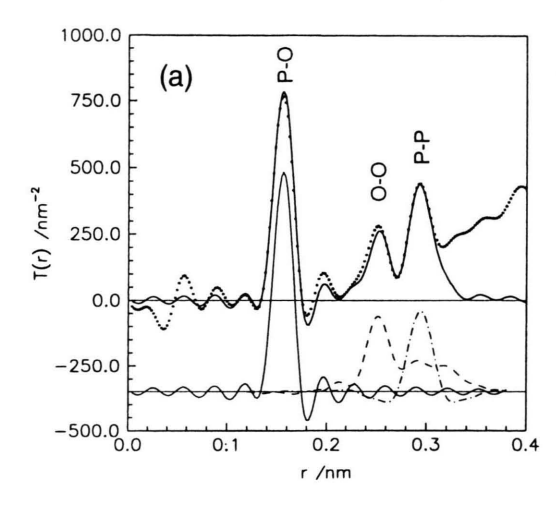
 ρ_0 is the number density of atoms. Gaussian functions were used as the model peaks. The termination effect of the Fourier transformation which is caused by the upper limit of the measuring range, $Q_{\text{max}} = 470 \text{ nm}^{-1}$ and 202 nm⁻¹ in the $S_N(Q)$ and $S_X(Q)$ data, was taken into account by folding the model peaks with appropriate peak functions [27]. This effect causes a broadening of the distance peaks and the occurrence of some satellite ripples. No modification function for their damping was applied. Such a damping causes an additional peak broadening. The parameters of the Gaussian functions of the first three nearest-neighbour peaks are given in Table 1. The procedure for extracting the parameters is described in [29]. The model peaks are shown in Figure 2b. The corresponding broadened peaks are plotted in Figure 2a. The appropriate sums of the broadened peaks are compared with the experimental $T_N(r)$ and $T_X(r)$ functions in Fig. 2, as well.

The parameters of the P-O and O-O peaks, which were already published in [6], are mainly determined by the $T_{\rm N}(r)$ data. The model peaks which are calculated by these parameters fit the $T_{\rm X}(r)$ function in the corresponding r-range, as well (Figure 2a). However, due to the small $Q_{\rm max}$ of the $S_{\rm X}(Q)$ data, the split P-O peak is not resolved in the $T_{\rm X}(r)$ function. Its two contributions cause only a slight asymmetry.

On the other hand, in the $T_{\rm X}(r)$ data the P-P peak is well resolved, where a coordination number, $N_{\rm PP}$, of three is expected for v-P₂O₅ [1–5]. But the fit of the full height of this peak by P-P contributions alone leads to unreasonably large $N_{\rm PP}$ values. Hence, this peak is not only formed from P-P contributions. In order to enable a meaningful fit, $N_{\rm PP}=3$ is fixed and some O-O distances are additionally introduced. At this stage of data evaluation it is not possible to differentiate the P-O and O-O

Table 1. Parameters of the Gaussian functions which model the nearest-neighbour peaks of ν -P₂O₅. fwhm is the full width at half maximum. The distances of the O-O_{2nd} neighbours are introduced to enable the fit of the P-P peak. The values marked by an asterisk are fixed during the fit.

Atom pair	Coordination number	Distance (pm)	fwhm (pm)	Total coordination number	Mean distance (pm)		
P-O	0.900 ± 0.1 3.050 ± 0.1	143.2 ± 0.5 158.1 ± 0.3	7 ± 2 10 ± 2	3.95 ± 0.1	154.7 ± 0.5		
0-0	1.75 ± 0.3 2.95 ± 0.3	243 ± 3 256 ± 3	16 ± 4 16 ± 4	4.7 ± 0.2	251 ± 2		
P-P	3.0*	294.2 ± 1.0	24 ± 5				
O-O _{2nd}	1.0* 3.5*	282* 315*	25* 45*				



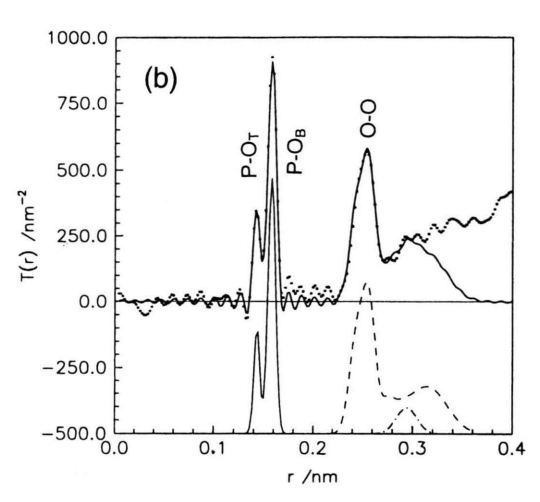
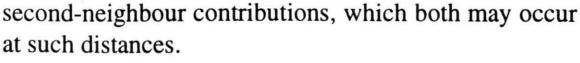


Fig. 2. Real-space correlation functions, $T_{\rm X}(r)$ and $T_{\rm N}(r)$, of the X-ray (a) and neutron (b) diffraction results: Comparison of the experimental curves (dotted lines) and the sums of the model peaks (solid lines) with the P-O, O-O, and P-P contributions (from the left to the right). In the lower part of the plots the original Gaussian functions (b) and the broadened peaks after folding with the peak functions (a) are shown: P-O – solid lines, O-O – dashed lines, P-P – dash-dotted lines.



Using the P-O_B bond length of (158.1 ± 0.3) pm and the P-P distance of (294.2 ± 1.0) pm, a mean of $137.0^{\circ}\pm3^{\circ}$ is obtained for the P-O-P bridging angle in ν -P₂O₅. The rmsd of the angular distribution of about 10° is simply determined by an estimation which exploits the fwhm of 24 pm for the P-P peak.

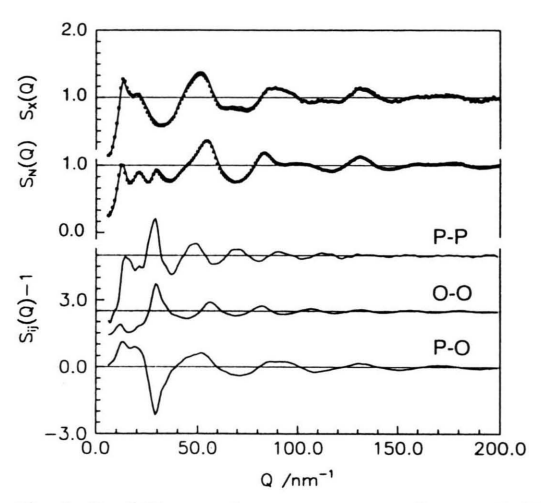


Fig. 3. Total X-ray and neutron structure factors, $S_X(Q)$ and $S_N(Q)$, and the three partials $S_{ij}(Q)$ of ν -P₂O₅ obtained from five RMC models (solid lines). The dotted lines are the experimental data. The curves are shifted vertically for clearness of the plot.

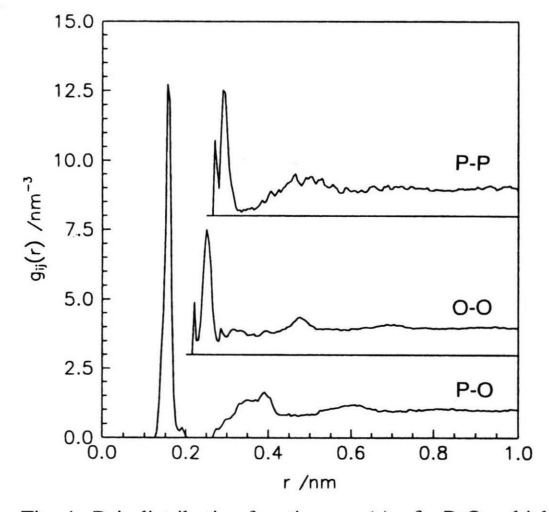


Fig. 4. Pair distribution functions, $g_{ij}(r)$, of v-P₂O₅ which correspond to the $S_{ij}(Q)$ functions in Figure 3. The curves are shifted vertically for clearness of the plot.

4.2. RMC Simulations of Vitreous P₂O₅

Although the use of two functions, $S_N(Q)$ and $S_X(Q)$, of different contrast is not sufficient for an exact separation into the partial $S_{ij}(Q)$ functions of the total S(Q) data of v- P_2O_5 , the three $S_{ij}(Q)$ functions resulting from the RMC simulations should feature the characteristics of the real partials. The agreement between the total mod-

el and experimental $S_N(Q)$ and $S_X(Q)$ data is good (Figure 3). The constraints, which are used as additional information and which are quoted in Sect. 3.2, guarantee the 3-dimensional RMC configurations to be sufficient for discussions on network features of v-P₂O₅. However, not the expected fraction of 60% but only 57% of the model O atoms are in bridging positions. All the other O atoms are in terminal positions. Thus, not all of the PO₄ units are threefold-linked. Some of them have only two links. The P-O peak at 155 pm is not split as found in the $T_{\rm N}(r)$ functions. In order to minimize the computing time, Q_{max} of the $S_{\text{N}}(Q)$ data used in the RMC simulations is equal to 255 nm⁻¹. An extension of this range does not naturally lead to models where the O_T and O_B atoms are correctly related with the short and the long P-O bond, respectively. Two of the three pair distributions, $g_{PP}(r)$ and $g_{OO}(r)$, show unreasonable spikes in front of the first real peak (cf. Figure 4). Thus, quantitative analyses of the RMC results need some care in order to separate slight shortcomings of the model configurations from intrinsic network characteristics of v-P₂O₅.

The contributions of the O-O and P-O correlations which are present at the position of the P-P peak and which were taken into account in the determination of its parameters (cf. Sect. 4.1) are clearly visible in the $g_{\rm OO}(r)$ and $g_{\rm PO}(r)$ distributions of the RMC simulations (cf. Figure 4). Actually, a direct extraction of the P-P coordination number from the $T_{\rm X}(r)$ data is not possible. The introduction of some O-O contributions is justified.

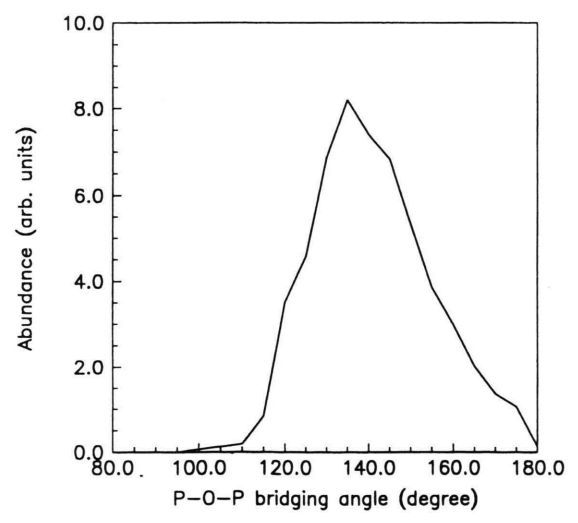


Fig. 5. Distribution of the P-O-P bridging angle of ν -P₂O₅ obtained from five RMC models.

The angular distribution of the P-O-P bridges, which is shown in Fig. 5, was obtained from the RMC models directly by calculating the P-O_B-P angle of each pair of linked PO₄ units. In order to avoid the influence of deficits of the network models, other than threefold-linked units were excluded from this procedure. The resulting mean angle of the distribution is equal to 140.9° with a rmsd of 14°. Thus, the distribution found in this way is broader and somewhat shifted toward larger angles than that which was directly obtained from the P-P distances (cf. Section 4.1).

The principal peak in the sense of Elliott's ideas [12], according to (1) is positioned at Q_p of about 50 nm⁻¹ in both S(Q) functions. This peak is related with the mean P-O bond length of 155 pm. The two or three "prepeaks" at Q_1 , Q_{1*} , and Q_2 of about 13, 20, and 29 nm⁻¹ in the $S_{\rm X}(Q)$ or $S_{\rm N}(Q)$ functions (Fig. 3) are, respectively, attributable to structures of larger dimensions, thus to the mutual order of the PO₄ tetrahedra. In general, the $S_{ii}(Q)$ functions of our RMC simulations (Fig. 3) resemble those of v-SiO₂ [30]. But for v-P₂O₅ the difference $Q_2 - Q_1$ is larger and the $S_{PO}(Q)$ function shows a clear shoulder at $Q_{1*} = 20 \text{ nm}^{-1}$, while peaks at this position are nearly not visible in the $S_{PP}(Q)$ and $S_{OO}(Q)$ functions. For v-SiO₂ the positions Q_1 and Q_2 are equal to 15 and 27 nm⁻¹ and the shoulder at Q_{1*} , occurring in the $S_{SiO}(Q)$ data, is small [30]. According to the similarity between the $S_{PP}(Q)$ data in Fig. 3 and the $S_{SiSi}(Q)$ function of v-SiO₂ [30], the same mechanism may be applied for explanation of the prepeaks at Q_1 and Q_2 (cf. Chapter 5). Hence, the assumption about sheets in the network structure of v-P₂O₅ [16] is not necessary for an understanding of the first peaks in $S_X(Q)$. No signs of two different P-P distances which belong to different network directions are detectable (Figs. 3 and 4). The main contribution to the prepeak at Q_{1*} , lying between both others, originates from the $S_{PO}(Q)$ data.

4.3. Comparison with the Three Crystalline Structures

A first attempt in the search for the structural origin of the prepeaks is usually made by a comparison with structures of the related crystals [14, 27]. Model structure factors of the three crystalline forms [17–19] were calculated according to (3). They do not sufficiently agree with the experimental $S_{\rm N}(Q)$ and $S_{\rm X}(Q)$ data. Only in case of the X-ray data the $S_{\rm mod}(Q)$ function of P_2O_5 , form II is similar to $S_{\rm X}(Q)$. In order to extract the origin of the differences between the structures of the crystals and the P_2O_5 glass, the partial $S_{\rm PP}(Q)$ and $T_{\rm PP}(r)$ model functions

Table 2. Comparison of structural parameters of the crystalline forms of P_2O_5 with those extracted from the RMC models of $v-P_2O_5$. Distances are given in pm. N_{OB} and N_{OT} are the numbers of O_B and O_T found at distances of r_{OB} and r_{OT} around an O_T atom. N_O is the sum of N_{OB} and N_{OT} . N_{P1} is the number of P neighbours at distances r_1 around a given P atom linked via a P-O_B-P₁ bridge. N_{P2} is the number of P_{2nd} neighbours at distances r_{P2} . Values marked by an asterisk belong to P_{2nd} neighbours which are connected via a P-O_B-P₁-O_B-P₂ linkage.

Structure (Crystal)	Density of atoms (nm ⁻¹)	P-O _B -P mean angle	O neighbours of the O _T atoms				P neighbours of the P atoms						
			$N_{\rm O}$	N_{OB}	N _{OT}	r _{OB}	r_{OT}	$N_{\rm P1}$	$r_{\rm Pl}$	N_{P2}	N _{P2*}	r _{P2}	r _{P2*}
P ₂ O ₅ , form I P ₂ O ₅ , form II P ₂ O ₅ , form III v-P ₂ O ₅ (RMC)	67.6 80.3 87.0 72.6	122.8° 131.5° 141.2° 140.9°	4.5 8 10 4.9	4.5 5 6 2.4	0 3 4 2.5	320 310 305 <340	325 315 <340	3 3 3 2.8	279 287 296 295	10.5 14.0 14.0 12.9	0 6 6 <6	493 485 461 490	487 480 495

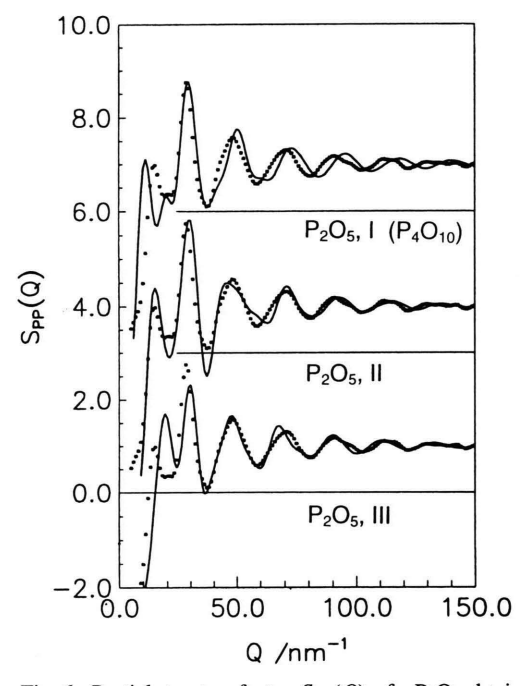


Fig. 6. Partial structure factor, $S_{PP}(Q)$, of $v-P_2O_5$ obtained from the RMC models (dots) in comparison with the $S_{PP}(Q)$ functions calculated for the three crystalline forms (lines). The curves are shifted vertically for clearness of the plot.

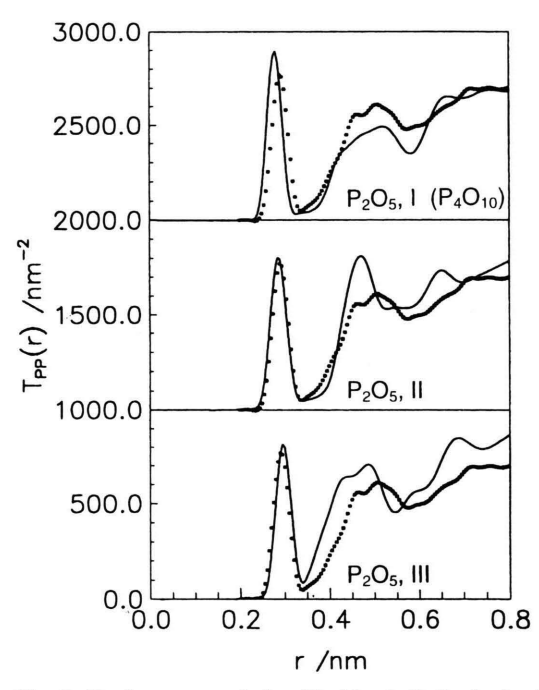


Fig. 7. Real-space correlation, $T_{\rm PP}(r)$, of v- P_2O_5 obtained from the RMC models (dots) in comparison with the $T_{\rm PP}(r)$ functions calculated for the three crystalline forms (lines). The curves are shifted vertically for clearness of the plot.

are compared with those resulting from the RMC simulations (cf. Figs. 6 and 7). Here the RMC data are considered as to be close to the real behaviour of the P_2O_5 glass network. The solid-lined $S_{PP}(Q)$ functions in Fig. 6 are calculated from the crystalline structures by (3) with z=0.04, L=0.55 nm and W=0.4 nm. The $T_{PP}(r)$ data in Fig. 7 are the Fourier transforms of $Q \cdot [S_{PP}(Q)-1]$, where all the $T_{PP}(r)$ functions were obtained using equal conditions.

The position of the first peak in the experimental S(Q) at Q_1 is well reproduced by the $S_{PP}(Q)$ data from the RMC

simulations (Figure 3). This position agrees only with that in the $S_{PP}(Q)$ of the P_2O_5 , form II crystal (Figure 6). In the real-space correlations, $T_{PP}(r)$, which are shown in Fig. 7, the positions of the P-P peak at 0.3 nm correlate with the P-O_B-P angle. Slight differences occur for the crystals P_2O_5 , forms II and III, but they become significant for P_4O_{10} , where the PO₄ units form threefold rings. The mean P-O_B-P angles of the glass and the crystals are compared in Table 2. Strong differences in the $T_{PP}(r)$ data of the glass and the crystals are visible at distances of 0.5 nm, where the second P neighbours along

the linked PO_4 units and other P neighbours via the non-linked side of the O_T atoms are expected. The numbers of such P_{2nd} neighbours and of O_T or O_B neighbours around an O_T in the crystalline structures and in the RMC models are also listed in Table 2. These values indicate that non of the three crystalline structures agrees well with the features of the glassy network.

5. Discussion

5.1. Short-range Structure

The present X-ray diffraction experiments confirm the knowledge [6] about the two different P-O bond lengths in v-P₂O₅. New information was obtained for distances between the P atoms which are linked via a common OB neighbour. A mean P-O_B-P angle of 137° ± 3° was calculated from this distance (294.2 pm) and that of the P-O_B bond (158.1 pm). The concerning angle in the RMC models was found to be about 141° with P-P distances and P-O_B lengths of 295 pm and 157.9 pm, respectively. The distance distributions of the RMC models are asymmetric. They have a tail on their right side and, thus, they differ from the Gaussian functions used in the fit of the T(r) data. This fact causes the differences between both angular distributions. Since the P-P peak shows an unrealistic spike at 275 pm (Fig. 4) we would not expect the mean angle of 141° to be more reliable than that of 137°. Note that the dominance of these angles excludes that a reasonable number of threefold rings can exist. Thus, P₄O₁₀ molecules can only play an unimportant role in v-P2O5.

Unlike the splitting of the P-O peak which is visible in the $T_{\rm N}(r)$ data (cf. Fig. 2b), the P-O peak from the RMC simulations is not split. Different from the expectations, some of the ${\rm O_B}$ belong to the short P-O bonds, and vice versa. An increase of $Q_{\rm max}$ in the fast Fourier transformation of the RMC simulations should result in the expected splitting. However, for an improvement of the relation of the ${\rm O_T}$ and the ${\rm O_B}$ with the short and the long P-O bond, respectively, it is required to introduce a new separation constraint for the P-O_B bond. Since the mean P-O_B bond length of the present RMC models is close to the value observed in the parameter fit, an increase of $Q_{\rm max}$ or a new constraint should not markedly alter the subsequent conclusions about the medium-range structure.

The O-O peak in the $T_{\rm N}(r)$ data (Fig. 2b) indicates the existence of two distances. From a comparison with the three crystalline structures [17–19] it was concluded [6]

that this effect is based on the existence of two different edges in the PO_4 unit, the O_B - O_B and the O_B - O_T edges. The first of edges is shorter by 8 pm. This corresponds to angles O_B -P- O_T of 116° and O_B -P- O_B of 102° . In both cases, the RMC simulations yield merely broad angular distributions with mean tetrahedral angles of 109° . Thus, the PO_4 units in the RMC models do not reflect all the known internal structural details. This shortcoming should not be essential for the subsequent, more qualitative discussion.

5.2. Medium-range Structure of the P Positions

At first, the positions of the "prepeaks" at Q_1 and Q_2 will be considered. Starting from a dense random packing of spheres, Dixmier [31] established a schematic hole model for amorphous Si with tetracoordinated atoms by removal of definite particles (cf. also [12]). This scheme is also valid for v-SiO₂ if only the Si positions are considered. The oxygen atoms which decorate the Si-Si links are neglected. Different from that principal peak which was defined in Chapt. 1, here the Si-Si distances produce their own principal peak which is positioned at Q_2 . The first coordination shell of a Si atom consists of four Si neighbours and several holes, which is illustrated in Figure 8. Since each of these four Si is linked with three other neighbours, twelve Si atoms are located in the second shell. Thus, the second shell appears densely packed. Hence it follows that this coordination shell produces the first scattering peak at Q_1 . According to (1), Q_1 corresponds to the Si-Si_{2nd} neighbour distance. In the Bhatia-Thornton formalism [32], this is the first peak in the concentration-concentration structure factor of Si atoms and voids [12, 31].

On account of the similarity between $S_{SiSi}(Q)$ and $S_{PP}(Q)$, this scheme is applied to $v-P_2O_5$. But a PO_4 unit

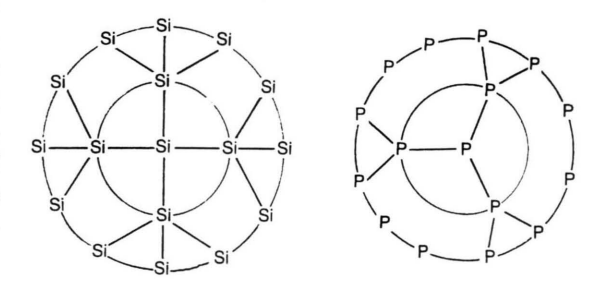


Fig. 8. Occupancy of the first coordination spheres (large circles) in ν -SiO₂ and ν -P₂O₅ around a Si (or P) atom. The lines denote Si(P)-O-Si(P) bridges.

has only three links. Thus, three P atoms are located in the first shell, and maximal six P neighbours, which are linked with a first shell P atom, form the second shell (Figure 8). Additionally, several other P neighbours are involved in the second shell which are not connected with the central P atom (cf. Table 2). The unlinked P neighbours cannot approach the P-P_{first} coordination shell of the central P atom. They are embedded among the linked PO₄ units in the second shell. Their number and positions are flexible. Obviously, the distance ratio of the P-P_{2nd} and P-P_{first} neighbours in ν -P₂O₅ is greater than that of the Si-Si_{2nd} and Si-Si_{first} neighbours in ν -SiO₂. For this reason the difference Q_2 - Q_1 is larger in the $S_{PP}(Q)$ data if compared with that in $S_{SiSi}(Q)$.

The number of linked P neighbours in the second shell is less than six if threefold rings occur in the network. To a minor extent this is found in our RMC models. The P_4O_{10} molecule represents an extreme case without any links to the second shell. In a schematic hole model [12, 31], however, it is not essential if there are links to the second shell or not. The large difference between the numbers of P neighbours in the first and the second shell, 3 and about 12, allows us to apply the model for the explanation of the peaks at Q_2 and Q_1 . Therefore, the first peak at Q_1 in the S(Q) data of v- P_2O_5 is related with a distance which belongs to network links as well as to a packing of unlinked PO_4 units. Until now, no details of the three crystals have been used for the understanding of the first diffraction peaks.

The variability of the first scattering peak in the $S_{\rm PP}(Q)$ data, as e.g. visible in Fig. 6, originates mainly from a different wise of packing of the unlinked PO₄ units. However, this packing develops in the limitations of the existing network links. In the P₄O₁₀ crystal the number of second P neighbours is small if compared with that in ν -P₂O₅ (Table 2) while the P-P_{2nd} distances are of almost equal value. In the crystal P₂O₅, form III eight unlinked P atoms are found at very short distances of about 450 pm. In P₂O₅, form II also eight such neighbours occur, but at about 485 pm (cf. Figure 7). Since this finding is very similar with that in the glass the Q_1 -positions of P₂O₅, form II and ν -P₂O₅ well agree (cf. Figure 6).

5.3. Structural Behaviour of the O Positions

In vitreous P_2O_5 the number of O neighbours around an O_T atom is, however, less than that in P_2O_5 , form II (Table 2). This difference may be connected with uneffective orientations of the PO_4 units in ν - P_2O_5 . As a consequence, the atomic number density in ν - P_2O_5 is less

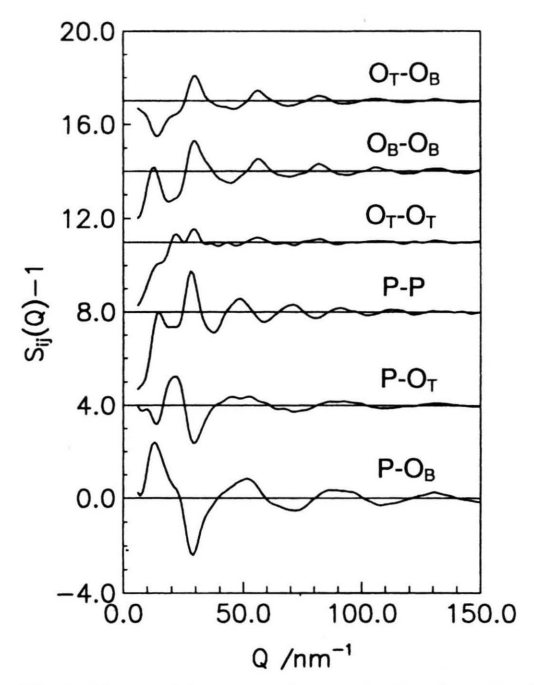


Fig. 9. The partial structure factors, $S_{ij}(Q)$, of $v\text{-P}_2\text{O}_5$ obtained from the RMC models. The O_T and O_B atoms are counted for different particles. The curves are shifted vertically for clearness of the plot.

than that in the crystal P_2O_5 , form II (cf. Table 2). The first neighbours of the O_T atoms in the crystals are several bridging oxygen atoms of the neighbouring PO_4 units at distances of 0.31 nm. In environments of a given O_T of the crystals P_2O_5 , form II and III additionally a small number of O_T atoms occurs at slightly larger distances. The unlike affinity with the O_B and O_T atoms may result from slight differences in their negative charge. In our RMC models of P_2O_5 glass both types of O atoms occur in the O_T environments by equal frequency. At this point it is not possible to decide whether this finding results from the inherent disorder of the P_2O_5 glassy network or from the disorder which is introduced by the reverse Monte Carlo approach.

The origin of the scattering peak at Q_{1*} is mainly related with the O_T atoms. For this purpose the O_B and O_T atoms are differentiated in the analysis of a RMC model. Partial $S_{ij}(Q)$ functions are obtained where both types of the O atoms are assumed to be different. The fraction of O_T atoms in the model exceeds by 3% the expected value of 40%. Therefore, only one O atom per P atom is denoted as an O_T . The few other terminal oxygen atoms are counted for an O_B . This shortcoming should not alter the conclusions made. The six resulting $S_{ij}(Q)$ functions

tions are shown in Figure 9. The main contribution to the peak at $20~\text{nm}^{-1}~(Q_{1^*})$ is attributable to the P-O_T correlations. Some little effects are visible in other correlations, among them in the P-O_B data. This finding must be explained by differences in the behaviour of the O_T and O_B atoms in the environments of the P atoms.

According to (1), the peak in the $S_{PO}(Q)$ data at 21 nm⁻¹ corresponds to a P-O distance of 0.37 nm. Actually, a broad P-O peak is located at this position (cf. Figure 4). Analysing a RMC model the numbers of O_T and O_B neighbours in this peak are obtained with about six and seven, respectively. Six of the seven O_B atoms belong to PO₄ units which are linked with the central P atom while only three of the six neighbouring O_T atoms belong to such tetrahedra. This situation is plotted in Fig. 10 which simply extends Fig. 8 by addition of the oxygen positions. According to the schematic hole model [12, 31] which was applied above we suggest: The 13 O atoms in the P-O_{2nd} shell produce an own scattering peak because the P-Ofirst shell contains only four O atoms. Several O_T neighbours and a few O_B atoms belong to PO₄ units which approach the central unit not by links but due to packing effects. These O_T and O_B atoms in the P-O_{2nd} shell behave like those of a first coordination shell (dashed-lined distances in Figure 10). Moreover, the O_T atoms are mainly found at short P-O_{2nd} distances (0.35 nm) if compared with the P-P_{2nd} distances. These facts produce the strong scattering peak at $Q_{1*} \cong 21 \text{ nm}^{-1}$ which in the total S(Q) data appears beside that at Q_1 . Though the ratio of O atoms in the

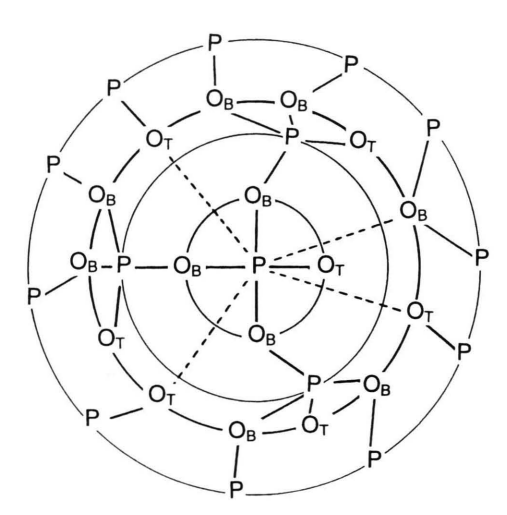


Fig. 10. Occupancy of the first coordination spheres around a Patom (large circles) in ν -P₂O₅. The full lines denote P-O bonds. The dashed lines denote those P-O_{2nd} distances whose O atoms do not belong to linked PO₄ units.

Si- O_{first} and Si- O_{2nd} shells in ν -SiO₂ is similar such flexible oxygen neighbours like those in the unlinked PO₄ units do not exist and, consequently, no separate peak at Q_{1*} is found but the concerning Si- O_{2nd} scattering contribution lies in the peak at Q_1 on its right side [30].

The O_T positions in the P- O_{2nd} shell of non-linked PO₄ units can partially be compared with those of the metal atoms (Me) in modified phosphate glasses. The first peaks in the $S_{MeP}(Q)$ functions of the glasses KPO₃ [33] and LaP₃O₉ [34] resemble that in the $S_{PO}(Q)$ data at 21 nm⁻¹ which is due to the agreement of the values r_{MeP} with the P-O_{2nd} distances. Due to the ionicity of the P-O bond the O_T are negatively, the P atoms are positively charged. The charge of an O_B atom is somewhat screened as it is positioned between two P neighbours. Thus, the ionic P-O_{2nd} interactions with the O_T atoms can contribute to the stability of the network. However, this is an effect in the second shell. It should be small.

A complete analysis of the first scattering peaks would require to look at the environments of the O atoms, as well. The O_B - O_B correlations follow the behaviour of the $S_{PP}(Q)$ data (Figure 9). The O_T - O_T correlations, however, seem to possess no significant order.

The scattering peak at 20 nm^{-1} retains up to an incorporation of about 20 mol% MeO [7]. Starting from $v\text{-P}_2\text{O}_5$ the twofold-linked PO₄ units formed are confronted with an orientational problem [35]. Their two O_T atoms cannot well coordinate the modifier cations in their isolated positions. Hence, their environments preserve somewhat that behaviour which was described above and which produces the scattering effect at 20 nm^{-1} . Approximately at a composition of 20 mol% modifier oxide content the orientational defect is improved [35] due to the increased number of modifier positions.

A further question arises which concerns the behaviour of scattering peaks for such glassy networks of basic structural units which are likewise threefold-linked. The neutron scattering intensities of v-As₂O₃ show also a peak at Q_{1*} while those of B₂O₃ do not [15]. But in the networks of both glasses no O_T atoms are involved. Therefore, it would be of great interest to analyse models of As₂O₃ networks to clarify the origin of the peak at Q_{1*} for this similar network glass.

The inspection of the RMC models reveals the occurence of extended network cages. If compared with ν -SiO₂ the dimensions of rings become large due to the existence of only three links per PO₄ unit. The concerning connectivity polyhedra possess flattened shapes. A few of such flattened cages positioned adjacent with each other produce structures which look like sheets stacked parallely.

A similar observation was made [36] in models of v-As₂O₃ [37]. However, it was outlined above that such network sheets are not necessary to explain the first peaks in the scattering intensities. Our finding does not concern those sheets of high atomic occupancy which Gaskell and Wallis [14] have detected in models of v-SiO₂. Their finding is a phenomenon which may occur separately from the existence of network sheets.

There is little prospect to gain further experimental information about the structure of ν -P₂O₅. By use of the new correlation techniques of the ³¹P NMR the knowledge about the P-O_B-P angular distribution may be improved. Our efforts in modelling ν -P₂O₅ will be continued by a control of the different behaviours of O_T and O_B atoms. But the RMC technique has its limitations. It is not possible to overcome all the problems by help of sophisticated constraints and it arises the question about the correct differentiation of inputs and results.

6. Conclusions

The present X-ray diffraction experiments on $v\text{-}P_2O_5$ confirmed the P-O distances which were recently obtained by neutron diffraction of high real-space resolution. A new result is the mean P-P distance of (294 ± 2) pm, which belongs to pairs of corner-linked PO₄ units. From the known distances, a mean P-O-P angle of $137^\circ \pm 3^\circ$ has been calculated.

The reverse Monte Carlo simulations were successful in reproducing the neutron and X-ray structure factors. The partial structure factors, among those where terminal and bridging oxygen atoms were differentiated, have

been used to correlate the first diffraction peaks with the occupancy and the distances of the first and second coordination shells around the P atom. The low occupancy of the first shells allows the application of the hole model of Dixmier. Different from the network of v-SiO₂, where all the atoms in the second shells are connected by a few bonds with the central Si atom, the model structures of v-P₂O₅ reveal the additional role of packing effects in these shells. The diffraction peak at 13 nm⁻¹ is related with the P-P_{2nd} shell. The shoulder at 20 nm⁻¹ arises from the P-O_{2nd} shell where the terminal oxygen atoms play the critical role. Not any of the related crystal structures is needed to describe the medium-range order of v-P₂O₅. Future work should have the aim to analyse the network cages formed by the rings of linked PO4 units.

The most similar crystalline form with vitreous P_2O_5 is the orthorhombic structure P_2O_5 , form II. It has, however, more effectively orientated terminal oxygen atoms and, thus, a higher packing than the glass. The existence of P_4O_{10} molecules can be excluded due to their unsuitable P-O-P angles. The crystal P_2O_5 , form III has the highest packing with short $P-P_{2nd}$ distances due to the unlinked PO_4 units mostly approaching the central P atom

Acknowledgements

The financial support of the Bundesministerium für Bildung und Forschung (Grant 03-KR4ROK-1) is gratefully acknowledged. Thanks are expressed to the Computing Service Center of the Rostock University for extensively provided computing time.

- [1] F. L. Galeener and J. C. Mikkelsen, Solid State Commun. 30, 505 (1979).
- [2] R. K.Brow, D. R. Tallant, J. J. Hudgens, S. W. Martin, and A. D. Irwin, J. Non-Cryst. Solids 177, 221 (1994).
- [3] J. J. Hudgens and S. W. Martin, J. Am. Ceram. Soc. 76, 1691 (1993).
- [4] K. Meyer, H. Hobert, A. Barz, and D. Stachel, Vibr. Spectr. 6, 323 (1994).
- [5] K. Meyer, A. Barz, and D. Stachel, J. Non-Cryst. Solids 191, 71 (1995).
- [6] U. Hoppe, G. Walter, A. Barz, D. Stachel, and A. C. Hannon, J. Phys.: Condens. Matter 10, 261 (1998).
- [7] G. Walter, U. Hoppe, T. Baade, R. Kranold, and D. Stachel, J. Non-Cryst. Solids 217, 299 (1997).
- [8] R. L. McGreevy and L.Pusztai, Molec. Simul. 1, 359 (1988).
- [9] A. K. Varshneya, R. F. Busbey, and T. F. Soules, J. Non-Cryst. Solids 69, 381 (1985).

- [10] G. Cormier, J. A. Capobianco, and A. Monteil, J. Non-Cryst. Solids 168, 115 (1994).
- [11] S. C. Moss and D. L. Price, in: Physics of disordered Materials, eds. D. Adler, H. Fritzsche and S. R. Ovshinsky, Plenum Press, New York 1985.
- [12] S. R. Elliott, J. Non-Cryst. Solids 182, 40 (1995).
- [13] P. S. Salmon, Proc. Roy. Soc. London A445, 351 (1994).
- [14] P. H. Gaskell and D. J. Wallis, Phys. Rev. Lett. 76, 66 (1996).
- [15] A. C. Wright, R. A. Hulme, D.I. Grimley, R. N. Sinclair, S. W. Martin, D. L. Price, and F. L. Galeener, J. Non-Cryst. Solids 129, 213 (1991).
- [16] G. Walter, U. Hoppe, R. Kranold, and D. Stachel, Phys. Chem. Glasses 35, 245 (1994).
- [17] D. Stachel, I. Svoboda, and H. Fuess, Acta Crystallogr. C51, 1049 (1995).
- [18] M. Jansen and B. Luer, Z. Kristallogr. 177, 149 (1986).

- [19] El. H. Arbib, B. Elouadi, J. P. Chaminade, and J. Darriet, J. Solid State Chem. 127, 350 (1996).
- [20] J. Blétry, Z. Naturforsch. 33a, 327 (1978).
- [21] K. Meyer, A. Barz, and D. Stachel, J. Non-Cryst. Solids 191, 71 (1995).
- [22] K. Meyer, A. Barz, and D. Stachel, in: Proc. 5th Int. Otto Schott Coll., Jena 1994, Glastechn. Ber. Glass Sci. Technol. 67C, 560 (1994).
- [23] K. Zickert, thesis, University of Rostock Germany 1988.
- [24] J. Krogh-Moe, Acta Crystallogr. 9, 951 (1956).
- [25] J. A. Ibers, and W. C. Hamilton (Eds), in: International tables for X-ray crystallography, Vol IV, Kynoch Press, Birmingham 1974, p. 71 ff.
- Birmingham 1974, p. 71 ff. [26] V. H. Smith jr., A. J. Thakkar, and D. C. Chapman, Acta Crystallogr. A31, 391 (1975).
- [27] A. J. Leadbetter and A. C. Wright, J. Non-Cryst. Solids 7, 23 (1972).
- [28] R. L. McGreevy, M. A. Howe, and J. D. Wicks, in: RMCA Version 3 – A General Purpose Reverse Monte Carlo Code, Studsvik (Sweden) October 1993.

- [29] U. Hoppe, G. Walter, D. Stachel, A. Barz, and A. C. Hannon, Z. Naturforsch. 52a, 259 (1997).
- [30] J. D. Wicks, PhD thesis, University of Oxford 1993.
- [31] J. Dixmier, J. Phys. I Paris 2, 1011 (1992).
- [32] A. B. Bhatia and D. E. Thornton, Phys. Rev. **B2**, 3004 (1970).
- [33] U. Hoppe, G. Walter, D. Stachel, and A. C. Hannon, Ber. Bunsenges. Phys. Chem. 100, 1569 (1996).
- [34] U. Hoppe, R. Kranold, D. Stachel, A. Barz, and A. C. Hannon, J. Non-Cryst. Solids, in press.
- [35] U. Hoppe, J. Non-Cryst. Solids 195, 138 (1996).
- [36] A. G. Clare, A. C. Wright, R. N. Sinclair, F. L. Galeener, and A. E. Geissberger, J. of Non-Cryst. Solids 111, 123 (1989).
- [37] D. Beeman, R. Lynds, and M. R. Anderson, J. Non-Cryst. Solids 42, 61 (1980).